Electronic Supplementary Material (ESI) for Sensors & Diagnostics.

Supplementary Information

Rapid quantification of the ethanol content in aqueous solutions using a ratiometric fluorescent sensor

Tianruo Shen, Davin Tan, Meyammai Shanmugham and Xiaogang Liu*

Fluorescence Research Group, Singapore University of Technology and Design (SUTD), 8 Somapah Road, Singapore 487372, Singapore

*Corresponding author: Xiaogang Liu (xiaogang_liu@sutd.edu.sg)

Contents

1. Comparison with alternative ethanol detection techniques

The following reported methods, including titration,[1,2] densitometry,[3,4] spectrophotometry,[5-8] gas chromatography (GC),[9-11] high-performance liquid chromatography (HPLC),[12,13] electrochemistry,[14-16] discoloration,[17,18] and fluorescence,[19-24] for qualifying the ethanol concentration were compared and briefly discussed in Table S1.

Table S1 Discussion of the reported techniques.

No	Reference	Basic Principle	Remarks
1	Fisher[1]	Titration	Golden standard method, high generalizability, requires specific instrument and operation process, uses toxic reagents
2	Nogueira *et al*[2]	Titration	Detection range (0~50% v/v), foldable paper-based analytical device, convenient operation, requires specific fabrication
3	Danahy *et al*[3]	Densitometry	Detection range (0~100% w/w), *in-situ* system control, requires special equipment and operation procedures
4	Li *et al*[4]	Densitometry	Detection range (48~78% v/v), novel hops image-based detection, uses artificial intelligence algorithm, requires special equipment and specific operation procedures
5	Abreu *et al*[5]	Spectrophotometry	Detection range (4~24% v/v), fast response, minimal sample consumption, commercially available chemical materials, requires specific operation procedures
6	Choengchan *et al*[6]	Spectrophotometry	Detection range (0.5~30% v/v), uses commercially available chemical materials, reduces sample

			contamination, requires specific operation procedures
7	Fletcher and Van Staden[7]	Spectrophotometry	Detection range (0~6% v/v), uses commercially available chemical materials, uses minimal regents, requires specific operation procedures
8	Sriariyanun *et al*[8]	Spectrophotometry	Detection range (0.7~8% v/v), fast response, uses commercially available chemical materials, encounters low solubility of the probe
9	Tiscione *et al*[9]	GC	Detection range (0.01~1 g/dL), high sensitivity and selectivity, minimal sample consumption, requires considerable testing time
10	Buckee and Mundy[10]	GC	Detection range (0.93~6.05% v/v), high sensitivity, minimal sample consumption, high reproducibility, requires specific analytical tools
11	Wasfi *et al*[11]	GC	Detection range (5~200 mg/dL), high sensitivity, minimal sample consumption, requires considerable testing time and specific operation procedures,
12	López and Gómez[12]	HPLC	Detection range (0.5~10% v/v), commercially available chemical materials, high reproducibility, needs a large amount of regents, requires specific operation procedures
13	Yarita *et al*[13]	HPLC	Detection range (1~2% v/v), low-cost reagents, commercially available chemical materials, high accuracy, requires considerable testing time and specific operation procedures

14	Bueno and Paixao[14]	Electrochemistry	Detection range (75~90% v/v), fast response, high sensitivity, requires specific fabrication and analytical tools
15	Shan *et al*[15]	Electrochemistry	Detection range (25~200 μM), fast response, high sensitivity, requires specific fabrication
16	Cinti *et al*[16]	Electrochemistry	Detection range (0~5% v/v), paper-based sensor, fast response, minimal sample consumption, requires specific fabrication
17	Yu *et al*[17]	Discoloration	Detection range (0~40% v/v), reusable indicator, fast response, straightforward evaluation, requires specific synthetic routes and operation procedures
18	Shahvar *et al*[18]	Discoloration	Detection range (98~99.5% v/v), smartphone-based detection, minimal sample consumption, requires toxic regents
19	Sharma and Quantrill[19]	Fluorescence	Detection range (0~40 mM), commercially available chemical materials, involves chemical reactions, requires considerable testing time and specific analytical tools
20	Hu *et al*[20]	Fluorescence	Detection range (0~100% v/v), ratiometric detection, high sensitivity, requires specific synthetic routes
21	Passos *et al*[21]	Fluorescence	Detection range (0~10% w/w), uses commercially available fluorophore, requires accurately controlled probe concentration for absorbance/emission intensity measurement, or expensive instrumentation for lifetime measurement

22	Jung *et al*[22]	Fluorescence	Detection range (60~90% v/v), ratiometric detection, smartphone-based detection, provides fast response, experiences low solubility of the probe, requires specific synthetic routes with toxic materials
23	Yin *et al*[23]	Fluorescence	Detection range (0~100% v/v), real-time detection, ratiometric detection, requires specific synthetic routes with toxic chemical agents
24	Fang *et al*[24]	Fluorescence	Detection range (0~100% v/v), film-based sensor, fast response, reduces sample contamination, requires specific synthetic routes

2. Experimental and computational methods

Chemical Materials

Table S2 Details of chemicals for the experiments.

No.	Name	CAS No.	Company	Product No.
1	Acridine	260-94-6	Sigma-Aldrich	A23609
2	Acetonitrile	75-05-8	Sigma-Aldrich	271004
3	Glycerol ≥99% v/v	56-81-5	Sigma-Aldrich	G7757
4	Ethyl acetate	141-78-6	VWR	23881.293
5	Dimethylformamide	68-12-2	VWR	23466.298
6	Ethylene glycol ≥99% v/v	107-21-1	VWR	24041.297
7	Buffer pH = 4.00 ± 0.02	NA	VWR	32095.297
8	Buffer pH = 7.00 ± 0.02	NA	VWR	32096.291
9	Buffer pH = 10.00 ± 0.02	NA	VWR	32040.298
10	Ethanol 90% (v/v)	64-17-5	VWR	83811.360
11	1,4-Dioxane	123-91-1	TCI	D0860
12	Ethanol >99.9% v/v	64-17-5	TCI	CT04
13	Methanol >99.8% v/v	67-56-1	TCI	M0097
14	Dimethyl sulfoxide	67-68-5	TCI	D5293

The water used for the experiments was the ultrapure water purified by the Arium Comfort II Benchtop Water Purification System with Integrated UV Lamp (H2O-II-1-UV-T) from Sartorius Stedim Singapore Pte. Ltd.

Spectral measurements

The emission spectra were measured using Duetta Fluorescence and Absorbance Spectrometer from HORIBA Scientific. Temperatures were controlled and adjusted using EXT-400 Liquid Cooling System from Koolance Inc and TC1 Temperature Controller from Quantum Northwest Inc, respectively.

The emission spectra of acridine were collected at 355 nm of excitation wavelength at 100 μM dye concentrations (unless specifically stated) in 1,4-dioxane (Diox), ethyl acetate (EAC), acetonitrile (ACN), dimethylformamide (DMF), dimethyl sulfoxide (DMSO), ethanol (EtOH), methanol (MeOH), ethylene glycol (EG), water, different buffers, and different ethanol-water mixtures, respectively.

Computational methods

Density functional theory (DFT) and time-dependent density functional theory (TD-DFT) calculations were conducted in Gaussian 16 program.[25-27] We considered six functional with different Hartree-Fock exchange fractions (HF%),[28] including B3LYP (HF% = 20%),[29] PBE0 (25%),[30,31] PW6B95 (28%),[32] BMK (42%),[33] M06-2X (54%),[34] and ωB97XD (22~100%)[35] with the def2-SVP basis set.[36] Solvation effects were considered using the SMD solvent model and linear-response (LR) solvent formalism in water.[37-39] All the optimized geometries were confirmed at the local minimum of the potential energy surfaces (unless specifically stated) in the ground state (S_0), the first excited state (S_1), and the second excited state (S_2). The hole-electron distributions were visualized using Multiwfn and VMD software.[40,41]

3. Optical properties of acridine in different solvents

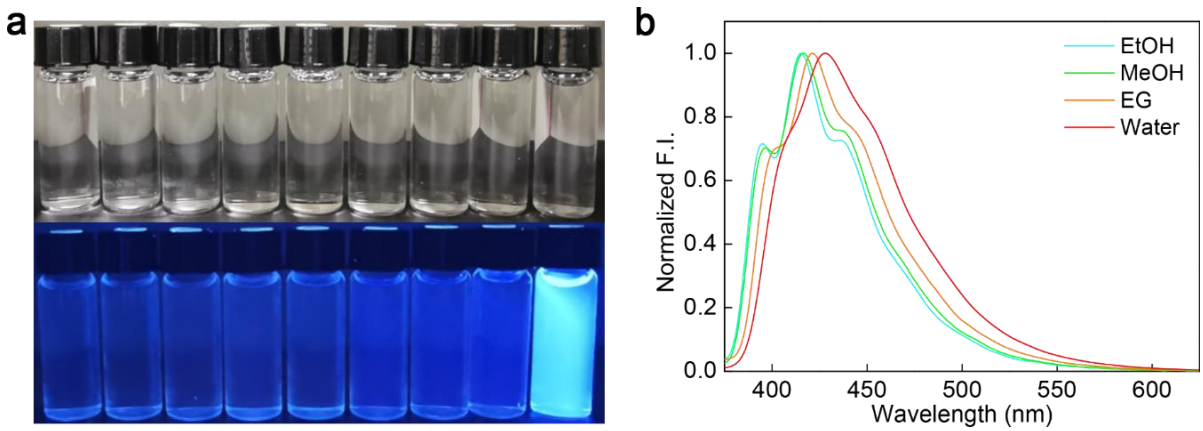

Fig. S1 (a) Samples of acridine in different solvents (acridine concentration = 100 μM). From left to right: Diox, EAC, ACN, DMF, DMSO, EtOH, MeOH, EG, and water under daylight (top) and UV light (bottom); (b) Normalized emission spectra of acridine in three alcohols and water.

Table S3 Dielectric constants (*ε*) of the solvents and the peak fluorescence intensity (F.I.) in these solvents.

No.	Solvent	*ε*	Peak F.I. (a.u.)
1	Diox	2.2099	19.19
2	EAC	5.9867	14.23
3	ACN	35.688	23.74
4	DMF	37.219	32.88
5	DMSO	46.826	41.00
6	EtOH	24.852	361.46
7	MeOH	32.613	472.13
8	EG	40.254	630.27
9	Water	78.3553	7567.97

4. Optical properties of acridine in EtOH-water mixtures under different temperatures and dye concentrations

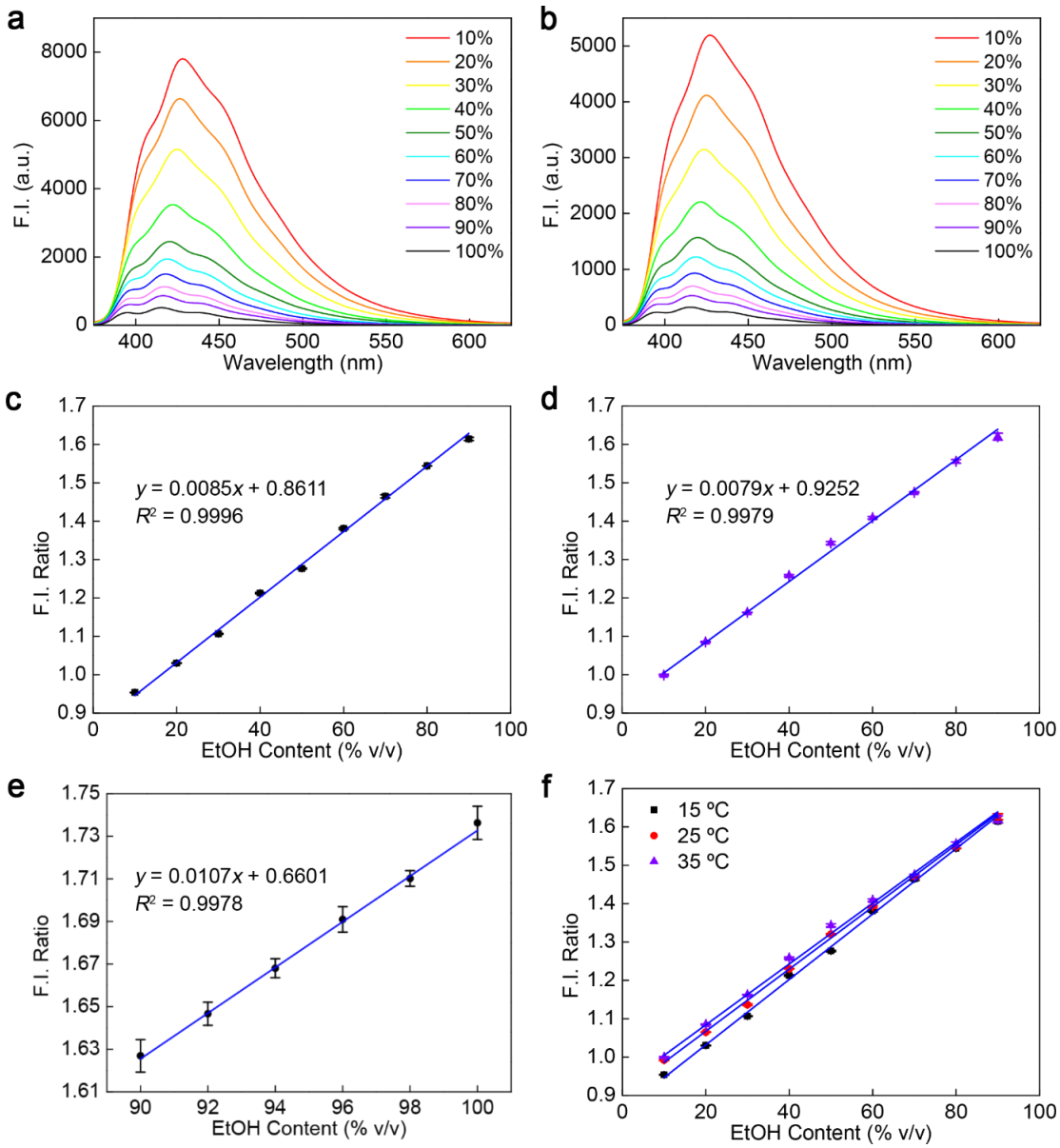

Fig. S2 Emission spectra of acridine in various EtOH-water mixtures at (a) 15 °C and (b) 35 °C; The EtOH content-dependence of fluorescence intensity (F.I.) ratios with linear fitting curves of acridine from 10~90% v/v EtOH content at (c) 15 °C and (d) 35 °C (The insets show the equations of the best linear fits); (e) The EtOH content-dependence of fluorescence intensity (F.I.) ratios of acridine from 90~100% v/v EtOH content with linear fitting curves of acridine (The insets illustrates the equations of the best linear fits) at 25 °C; (f) The EtOH content-dependence of fluorescence intensity (F.I.) ratios with linear fitting curves of acridine from 10~90% v/v EtOH content at different temperatures.

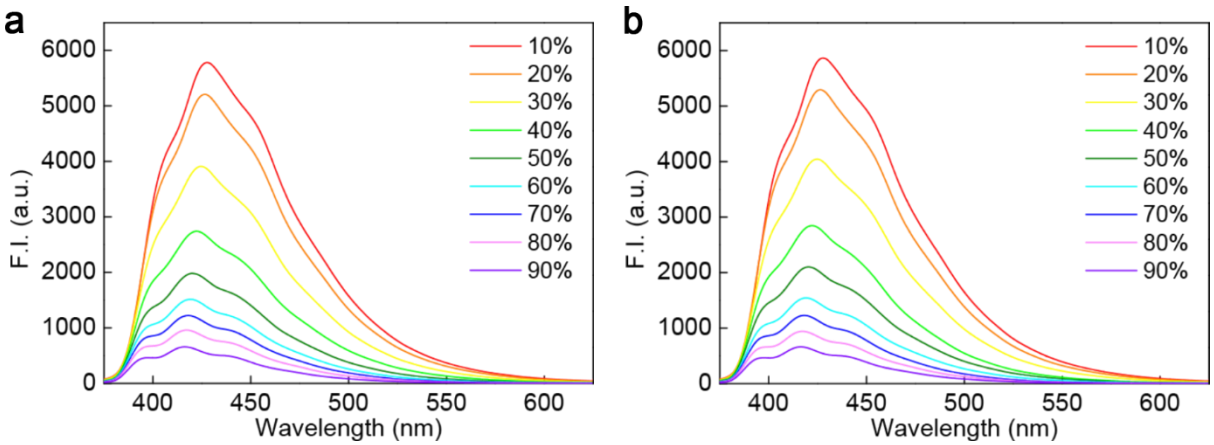

Fig. S3 Emission spectra of acridine in various EtOH-water mixtures with a dye concentration of (a) 110 μM and (b) 120 μM.

5. Investigating the effects of impurities and pH on the detection

Two ethanolic samples (the concentration of acridine = 100 μM) were prepared to assess the potential impact of the impurities. Sample 1 (the control sample) contains 75% v/v EtOH and 25% v/v water. In Sample 2 (the experimental sample), 1% v/v impurity (MeOH: EG: glycerol = 4:2:1 v/v/v) was dissolved in the mixture of 75% v/v EtOH and 24% v/v water. Our ratiometric method was applied for quantifying the EtOH concentration of each sample (Fig. 1c, S4, and S5).

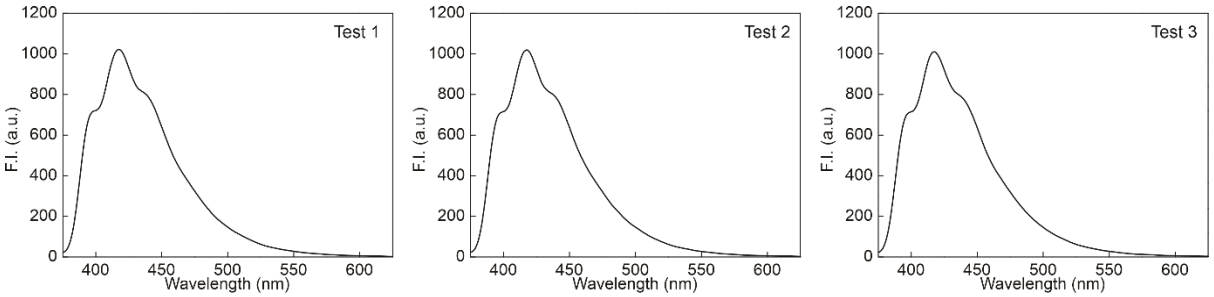

Fig. S4 Emission spectra of Sample 1 during three tests.

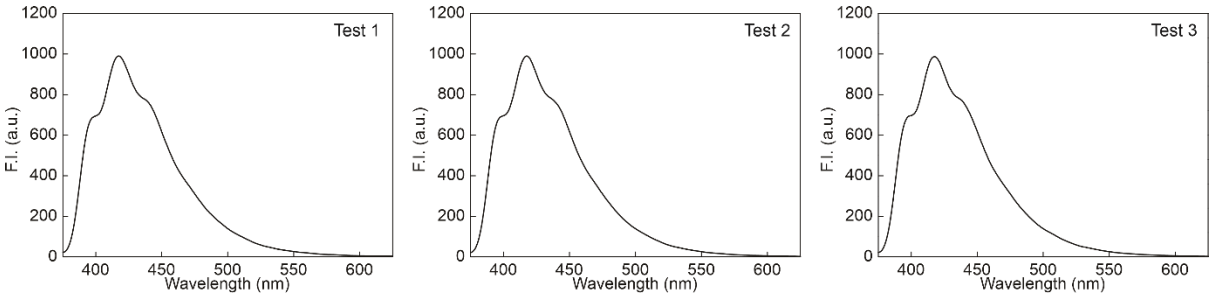

Fig. S5 Emission spectra of Sample 2 during three tests.

The results showed that the average measured values of Sample 1 and Sample 2 are 74.94% and 75.18%, respectively (Table S4). These experiments indicated that a small amount of impurities has minimal influence on the detection accuracy.

Table S4 Results of the measurements for Samples 1 and 2.

Sample	1			2		
Test	1	2	3	1	2	3
F.I. ratio	1.514	1.516	1.506	1.518	1.513	1.512
Equation	y = 0.0081x + 0.9052					
Concentration (% v/v)	75.22	75.45	74.15	75.69	75.00	74.86
Average (% v/v)	74.94			75.18		
Standard deviation	0.565			0.360		
Absolute error (%)	0.06			0.18		
Relative error (%)	0.08			0.25		

We also carried out the spectral measurements of acridine in various MeOH-water mixtures (Fig. S6). The results showed that the calibration to methanol is different from that of ethanol, illustrated by a different slope (0.0067).

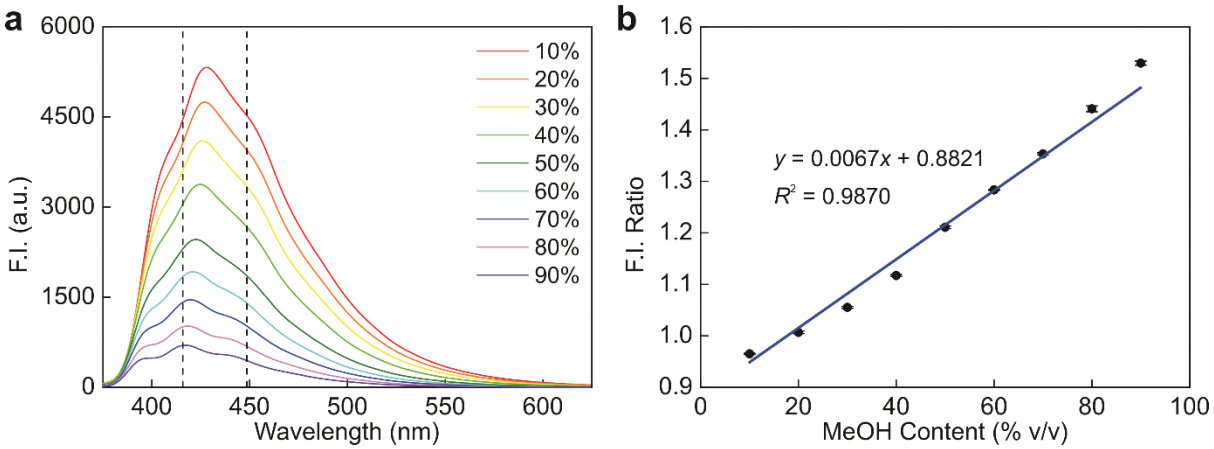

Fig. S6 (a) The emission spectra of acridine (100 μM) in various MeOH-water mixtures at 25 °C; the two dash lines highlight the fluorescence intensity (F.I.) at 415 nm and 448 nm, respectively; (b) The methanol content-dependence of F.I. ratios (the ratio of F.I. values at 415 nm and 448 nm) with corresponding linear fitting curve; the inset shows the best linear fitting equation.

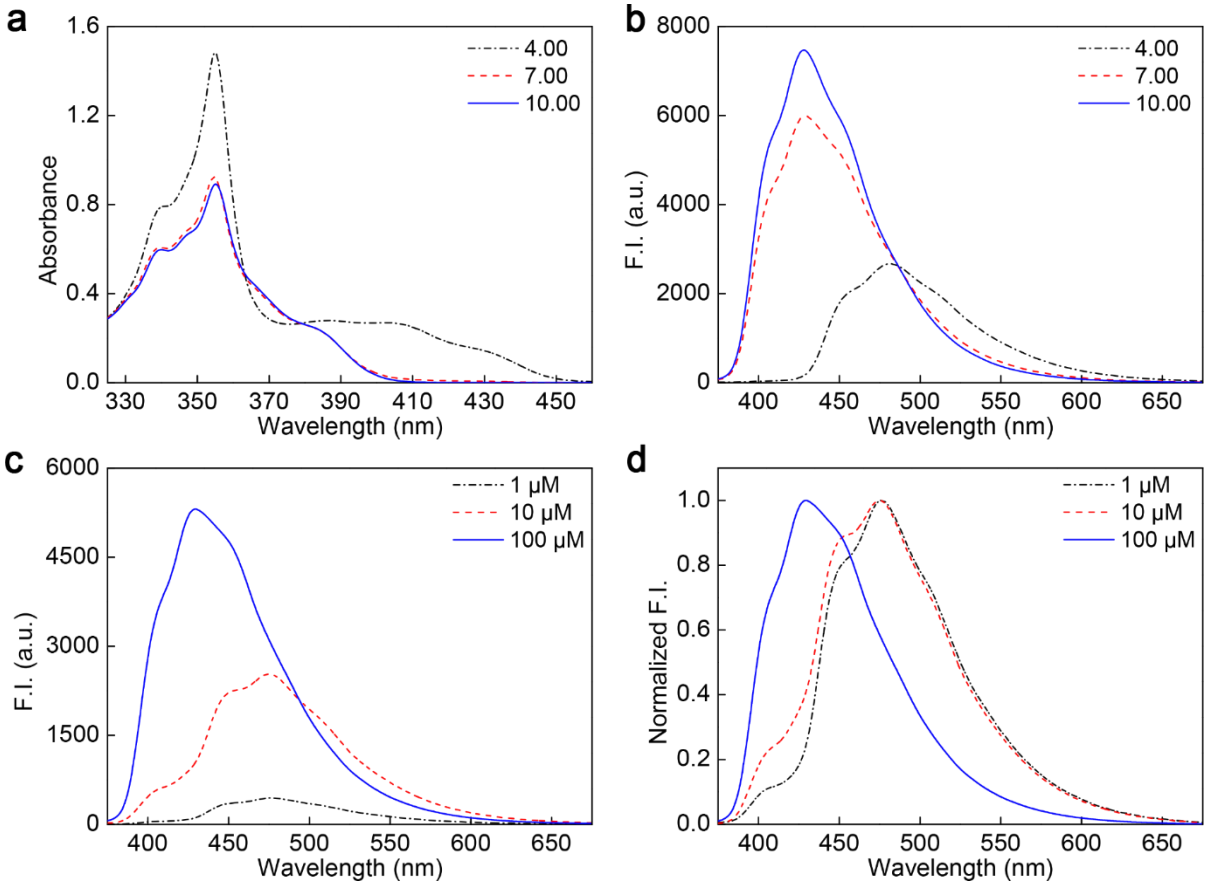

Fig. S7 (a) UV-vis absorption and (b) emission spectra of acridine in different buffers; (c) Emission and (d) normalized emission spectra of acridine with different dye concentrations in the pH ≈ 6.5 water.

6. Demonstration of the ratiometric method

We collected the emission spectra of acridine dissolved in EtOH purchased from VWR Singapore Pte Ltd, with the labelled concentration (90% v/v) (Fig. S5). We calculated the F.I. ratios between 415 nm and 448 nm and substituted the ratios into the linear fitting equation in Fig. 1c and S2e, as 90% v/v is a boundary value. Our results showed that this method has good reproducibility with low errors (Table S3).

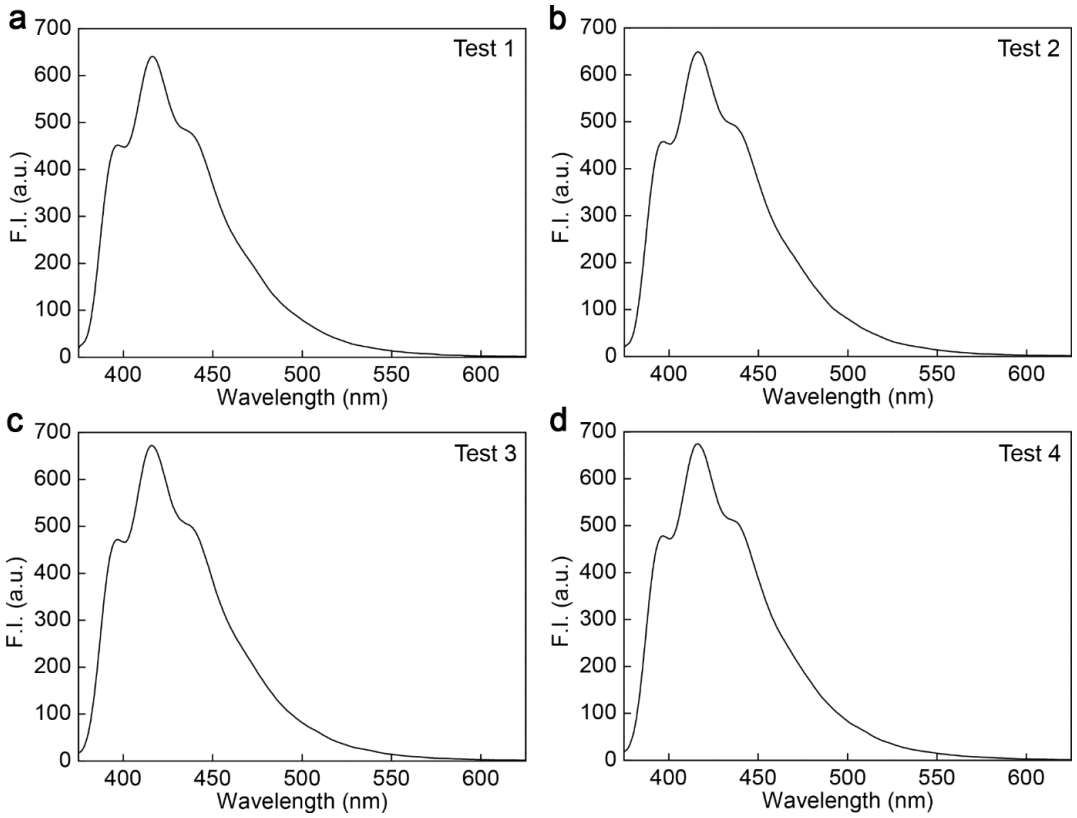

Fig. S8 Emission spectra of acridine dissolved into the calibrated EtOH solutions (90% v/v) from VWR for four testing times.

Table S5 Results of the measurement of calibrated 90% v/v ethanol using two linear fitting curves.

Test	1	2	3	4	1	2	3	4
F.I. ratio	1.623	1.625	1.631	1.626	1.623	1.625	1.631	1.626
Equation	$y = 0.0081x + 0.9052$				$y = 0.0107x + 0.6601$			
Concentration (% v/v)	88.67	88.92	89.55	88.95	89.77	89.96	90.44	89.99
Average (% v/v)	89.02				90.04			
Standard deviation	0.325				0.245			
Absolute error (%)	0.98				0.04			
Relative error (%)	1.08				0.05			

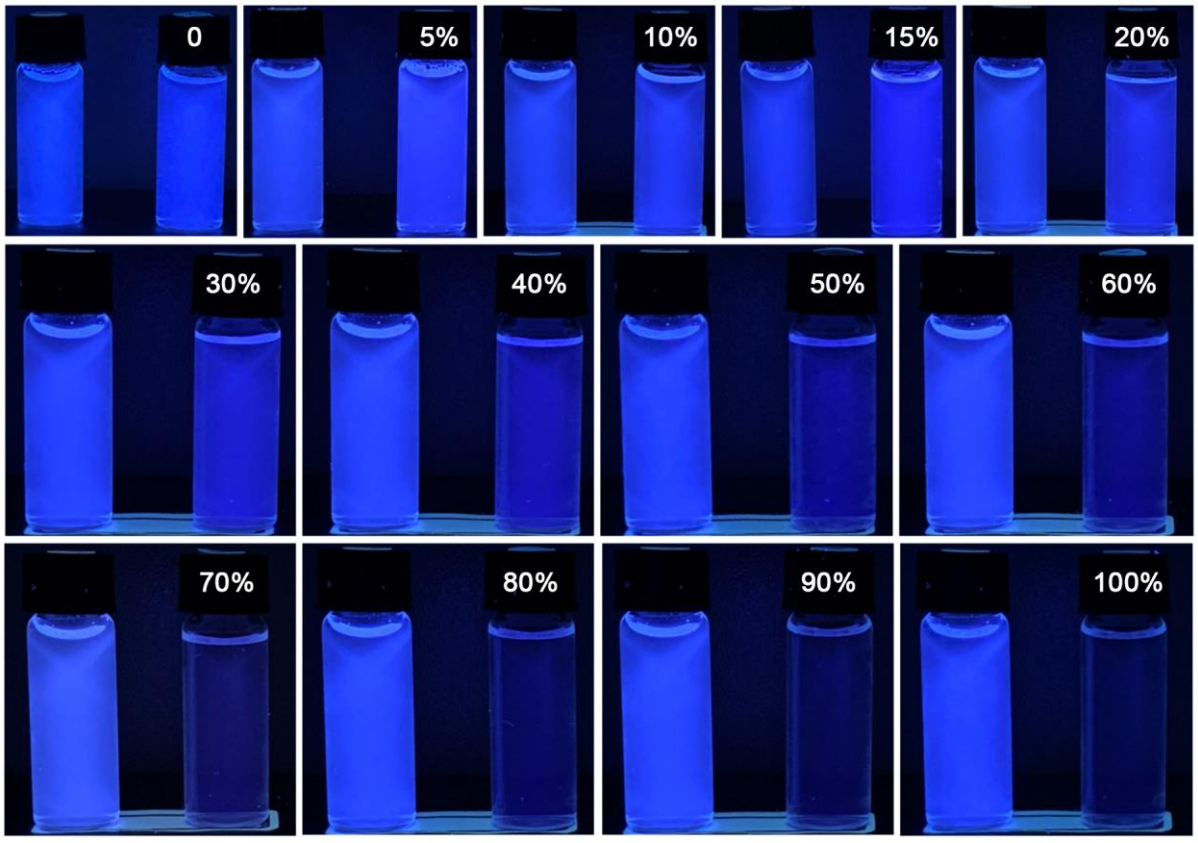

Fig. S9 Photographs of the reference acridine sample (left) and the known samples (right) with different EtOH contents under UV light (The inset shows the EtOH content of the solution in each vial). The images were captured using a normal smartphone.

Table S6 Intensity values of the blue and green channels from the photos of reference (left) and known (right) samples taken by the smartphone (Test 1).

Channel	Blue			Green		
EtOH content (% v/v)	Left	Right	Ratio	Left	Right	Ratio
0	254	255	1.004	65	65	1.000
5	254	253	0.996	75	69	0.920
10	243	239	0.984	65	56	0.862
15	244	242	0.992	70	54	0.771
20	244	228	0.934	66	47	0.712
30	254	201	0.791	68	33	0.485
40	254	180	0.709	70	27	0.386
50	254	153	0.602	68	18	0.265
60	253	132	0.522	72	13	0.181
70	250	111	0.444	88	29	0.330
80	254	96	0.378	73	13	0.178
90	254	77	0.303	73	8	0.110
100	255	64	0.251	64	8	0.125

Table S7 Intensity values of the blue and green channels from the photos of reference (left) and known (right) samples taken by the smartphone (Test 2).

Channel	Blue			Green		
EtOH content (% v/v)	Left	Right	Ratio	Left	Right	Ratio
0	254	253	0.996	63	64	1.016
5	255	255	1.000	76	69	0.908
10	238	236	0.992	65	55	0.846
15	249	243	0.976	73	57	0.781
20	244	231	0.947	66	47	0.712
30	253	201	0.794	66	35	0.530
40	255	178	0.698	68	25	0.368
50	255	143	0.561	67	16	0.239
60	254	129	0.508	73	15	0.205
70	251	106	0.422	89	24	0.270
80	254	94	0.370	75	12	0.160
90	253	77	0.304	72	10	0.139
100	253	66	0.261	63	10	0.159

Table S8 Intensity values of the blue and green channels from the photos of reference (left) and known (right) samples taken by the smartphone (Test 3).

Channel	Blue			Green		
EtOH content (% v/v)	Left	Right	Ratio	Left	Right	Ratio
0	253	252	0.996	63	63	1.000
5	254	254	1.000	73	68	0.932
10	244	239	0.980	66	57	0.864
15	247	245	0.992	73	60	0.822
20	242	234	0.967	64	49	0.766
30	254	204	0.803	67	35	0.522
40	254	179	0.705	70	23	0.329
50	254	147	0.579	66	14	0.212
60	255	130	0.510	71	13	0.183
70	250	100	0.400	88	22	0.250
80	255	93	0.365	74	11	0.149
90	254	78	0.307	73	8	0.110
100	253	63	0.249	61	8	0.131

Table S9 Average intensities of the blue and green channels from the photos of various samples taken by the smartphone.

Channel	Blue		Green	
EtOH content (% v/v)	Average	Standard derivation	Average	Standard derivation
0	0.999	0.004	1.005	0.007
5	0.999	0.002	0.920	0.010
10	0.985	0.005	0.857	0.008
15	0.987	0.008	0.791	0.022
20	0.949	0.013	0.730	0.025
30	0.796	0.005	0.513	0.020
40	0.704	0.004	0.361	0.024
50	0.581	0.017	0.239	0.021
60	0.513	0.006	0.190	0.011
70	0.422	0.018	0.283	0.034
80	0.371	0.005	0.162	0.012
90	0.305	0.002	0.119	0.014
100	0.254	0.005	0.138	0.015

Fig. S10 Picture of the reference sample (left; pure water) and the test sample (right; calibrated at 90% v/v ethanol solution) under UV light.

Table S10 The measurement results of calibrated 90% v/v ethanol using the smartphone method.

Test	1		2		3		4	
	Left	Right	Left	Right	Left	Right	Left	Right
Value of the blue channel	242	77	243	74	241	76	241	75
Ratio	0.318		0.305		0.315		0.311	
Concentration (% v/v)	88.35		90.05		88.70		89.22	
Average concentration (% v/v)	89.08							
Standard deviation	0.640							
Absolute error (%)	0.92							
Relative error (%)	1.02							

7. Computational analysis of the fluorescence mechanism

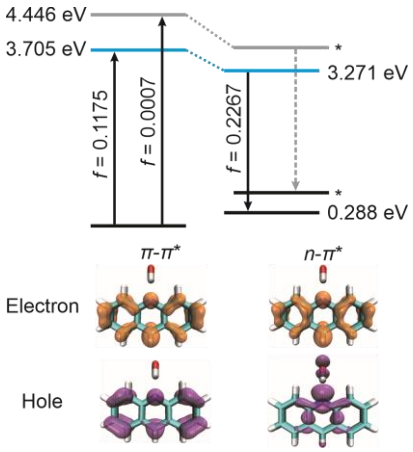

Fig. S11 Energy levels of the dark *n*-*π** and bright *π*-*π** states of acridine attached with an explicit water molecule during the excitation and emission progresses in water using the *ω*B97XD functional. The bottom row illustrates the hole-electron distributions during the vertical excitation (* means the state was not optimized).

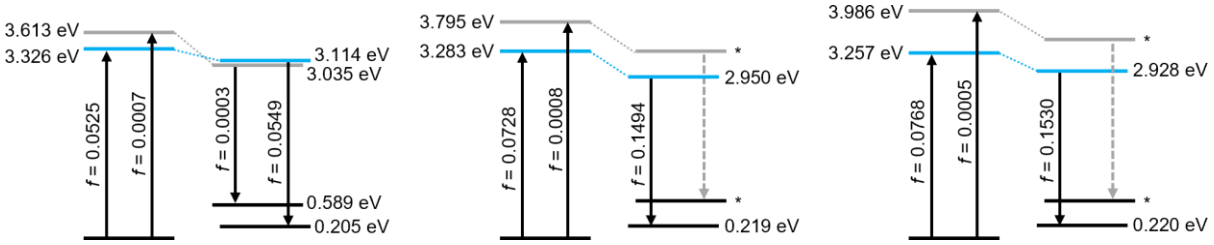

Fig. S12 The presence of the dark *n*-*π** state and bright *π*-*π** state of acridine during the vertical excitation and emission progresses in vacuum (left), water (middle), and a water molecule attaching to the acridine in water (right) using the B3LYP functional (* means the state was not optimized).

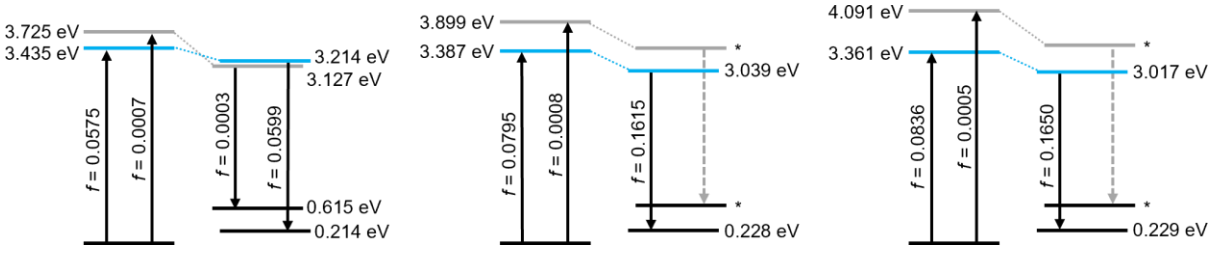

Fig. S13 The presence of the dark *n*-*π** state and bright *π*-*π** state of acridine during the vertical excitation and emission progresses in vacuum (left), water (middle), and a water molecule attaching to the acridine in water (right) using the PBE0 functional (* means the state was not optimized).

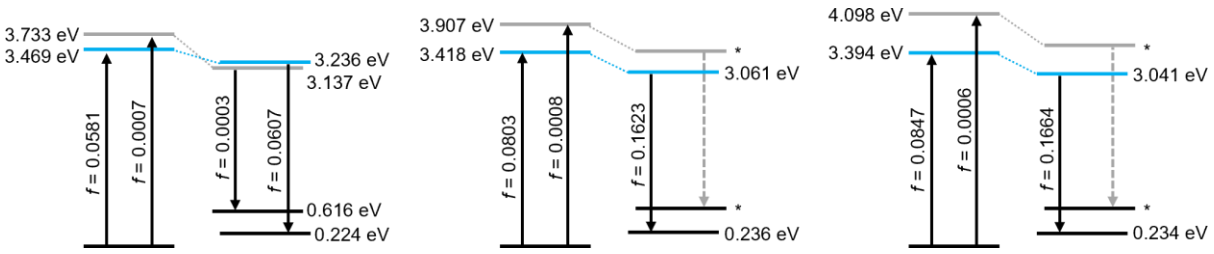

Fig. S14 The presence of the dark *n*-*π** state and bright *π*-*π** state of acridine during the vertical excitation and emission progresses in vacuum (left), water (middle), and a water molecule attaching to the acridine in water (right) using the PW6B95 functional (* means the state was not optimized).

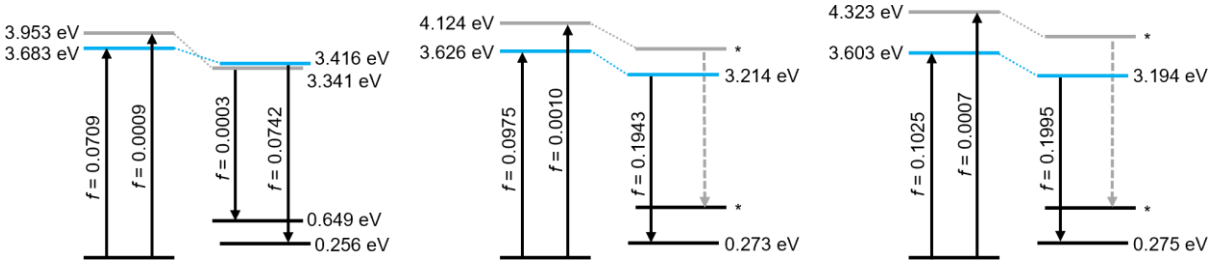

Fig. S15 The presence of the dark *n*-*π** state and bright *π*-*π** state of acridine during the vertical excitation and emission progresses in vacuum (left), water (middle), and a water molecule attaching to the acridine in water (right) using the BMK functional (* means the state was not optimized).

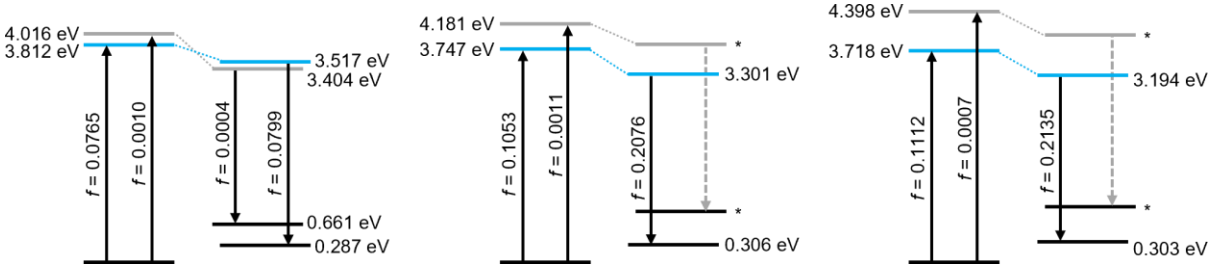

Fig. S16 The presence of the dark *n*-*π** state and bright *π*-*π** state of acridine during the vertical excitation and emission progresses in vacuum (left), water (middle), and a water molecule attaching to the acridine in water (right) using the M06-2X functional (* means the state was not optimized).

Table S11 Solvatochromic parameters[42, 43] of different solvents and optical properties[44] of acridine in these solvents.

Solvent	π^*	β	α	Peak λ_{em} (nm)	Quantum Yield (x10^3)
Hexane	-0.08	0	0	405	0.096
Benzene	0.59	0.1	0	410	0.33
DMF	0.88	0.69	0	410	0.028
ACN	0.75	0.31	0.19	410	0.35
2-Propanol	0.48	0.95	0.76	413	7.5
EtOH	0.54	0.77	0.83	415	7.9
MeOH	0.6	0.62	0.93	417	10.2
Formamide	0.97	0.48	0.71	420	9.7

Table S12 Results of the multiple linear regression analysis for the quantum yields of acridine in different solvents with corresponding coefficients to three solvatochromic parameters.

Regression Statistics		Coefficients	
Multiple *R*	0.978	Intercept	-0.362
R^2	0.957	π^*	1.376
Adjusted R^2	0.924	β	-2.100
Standard Error	1.292	α	11.907

8. References

1 K. Fischer, *Angew. Chem.*, 1935, **48**, 394-396.

2 S. A. Nogueira, A. D. Lemes, A. C. Chagas, M. L. Vieira, M. Talhavini, P. A. O. Morais and W. K. T. Coltro, *Talanta*, 2019, **194**, 363-369.

3 B. Danahy, D. Minnick and M. Shiflett, *Fermentation*, 2018, **4**, 72.

4 X. Li, J. Zhang, Y. Xue and L. Qiu, *Measurement*, 2022, **194**, 110955.

5 V. L.R.G. Abreu, J. L. M. Santos and J. L. F. C. Lima, *Food Anal. Methods*, 2011, **5**, 867-873.

6 N. Choengchan, T. Mantim, P. Wilairat, P. K. Dasgupta, S. Motomizu and D. Nacapricha, *Anal. Chim. Acta*, 2006, **579**, 33-37.

7 P. J. Fletcher and J. F. Van Staden, *Anal. Chim. Acta*, 2003, **499**, 123-128.

8 M. Sriariyanun, P. Mutrakulcharoen, S. Tepaamorndech, K. Cheenkachorn and K. Rattanaporn, *Orient. J. Chem.*, 2019, **35**, 744-750.

9 N. B. Tiscione, I. Alford, D. T. Yeatman and X. Shan, *J. Anal. Toxicol.*, 2011, **35**, 501-511.

10 G. Buckee and A. Mundy, *J. Inst. Brew.*, 1993, **99**, 381-384.

11 I. A. Wasfi, A. H. Al-Awadhi, Z. N. Al-Hatali, F. J. Al-Rayami and N. A. Al Katheeri, *J. Chromatogr. B: Anal. Technol. Biomed. Life Sci.*, 2004, **799**, 331-336.

12 E. F. López and E. F. Gómez, *J. Chromatogr. Sci.*, 1996, **34**, 254-257.

13 T. Yarita, R. Nakajima, S. Otsuka, T. Ihara, A. Takatsu and M. Shibukawa, *J. Chromatogr. A*, 2002, **976**, 387-391.

14 L. Bueno and T. R. Paixao, *Talanta*, 2011, **87**, 210-215.

15 C. Shan, H. Yang, D. Han, Q. Zhang, A. Ivaska and L. Niu, *Biosens. Bioelectron.*, 2010, **25**, 1504-1508.

16 S. Cinti, M. Basso, D. Moscone and F. Arduini, *Anal. Chim. Acta*, 2017, **960**, 123-130.

17 Y. Yu, S. Brandt, N. J. Nicolas and J. Aizenberg, *ACS Appl. Mater. Interfaces*, 2020, **12**, 1924-1929.

18 A. Shahvar, D. Shamsaei and M. Saraji, *Measurement*, 2020, **150**, 107068.

19 A. Sharma and N. S. M. Quantrill, *Spectrochim. Acta A: Mol. Spectrosc.*, 1994, **50**, 1161-1177.

20 X. Hu, H. Cao, W. Dong and J. Tang, *Talanta*, 2021, **233**, 122480.

21 W. E. Passos, I. P. Oliveira, F. S. Michels, M. A. G. Trindade, E. A. Falcão, B. S. Marangoni, S. L. Oliveira and A. R. L. Caires, *Renew. Energy*, 2021, **165**, 42-51.

22 Y.-u. Jung, M. G. Choi, S. H. Lee and S.-K. Chang, *Sens. Actuators B: Chem.*, 2017, **241**, 342-348.

23 H. Q. Yin, J. C. Yang and X. B. Yin, Anal. Chem., 2017, **89**, 13434-13440.

24 R. Huang, K. Liu, H. Liu, G. Wang, T. Liu, R. Miao, H. Peng and Y. Fang, *Anal. Chem.,* 2018, **90**, 14088-14093.

25 A. D. Becke, *J. Chem. Phys.*, 1993, **98**, 5648-5652.

26 G. Scalmani, M. J. Frisch, B. Mennucci, J. Tomasi, R. Cammi and V. Barone, *J. Chem. Phys.*, 2006, **124**, 94107.

27 M. J. Frisch, G. W. Trucks, H. B. Schlegel, G. E. Scuseria, M. A. Robb, J. R. Cheeseman, G. Scalmani, V. Barone, G. A. Petersson, H. Nakatsuji, X. Li, M. Caricato, A. V. Marenich, J. Bloino, B. G. Janesko, R. Gomperts, B. Mennucci, H. P. Hratchian, J. V. Ortiz, A. F. Izmaylov, J. L. Sonnenberg, D. Williams-Young, F. Ding, F. Lipparini, F. Egidi, J. Goings, B. Peng, A. Petrone, T. Henderson, D. Ranasinghe, V. G. Zakrzewski, J. Gao, N. Rega, G. Zheng, W. Liang, M. Hada, M. Ehara, K. Toyota, R. Fukuda, J. Hasegawa, M. Ishida, T. Nakajima, Y. Honda, O. Kitao, H. Nakai, T. Vreven, K. Throssell, J. A. Montgomery, Jr., J. E. Peralta, F. Ogliaro, M. J. Bearpark, J. J. Heyd, E. N. Brothers, K. N. Kudin, V. N. Staroverov, T. A. Keith, R. Kobayashi, J. Normand, K. Raghavachari, A. P. Rendell, J. C. Burant, S. S. Iyengar, J. Tomasi, M. Cossi, J. M. Millam, M. Klene, C. Adamo, R. Cammi, J. W. Ochterski, R. L. Martin, K. Morokuma, O. Farkas, J. B. Foresman, and D. J. Fox, Gaussian, Inc., Wallingford CT, 2016.

28 C. C. J. Roothaan, *Rev. Mod. Phys.*, 1951, **23**, 69-89.

29 A. J. Cohen and N. C. Handy, *Mol. Phys.*, 2001, **99**, 607-615.

30 C. Adamo and V. Barone, *J. Chem. Phys.*, 1999, **110**, 6158-6170.

31 A. V. Krukau, O. A. Vydrov, A. F. Izmaylov and G. E. Scuseria, *J. Chem. Phys.*, 2006, **125**, 224106.

32 Y. Zhao and D. G. Truhlar, *J. Phys. Chem. A*, 2005, **109**, 5656-5667.

33 A. D. Boese and J. M. Martin, *J. Chem. Phys.*, 2004, **121**, 3405-3416.

34 Y. Zhao and D. G. Truhlar, *Theor. Chem. Acc.*, 2007, **120**, 215-241.

35 J. D. Chai and M. Head-Gordon, *Phys. Chem. Chem. Phys.*, 2008, **10**, 6615-6620.

36 F. Weigend and R. Ahlrichs, *Phys. Chem. Chem. Phys.*, 2005, **7**, 3297-3305.

37 A. V. Marenich, C. J. Cramer and D. G. Truhlar, *J. Phys. Chem. B*, 2009, **113**, 6378-6396.

38 K. V. Mikkelsen, P. Jo/rgensen and H. J. r. A. Jensen, *J. Chem. Phys.*, 1994, **100**, 6597-6607.

39 M. Caricato, B. Mennucci, J. Tomasi, F. Ingrosso, R. Cammi, S. Corni and G. Scalmani, *J. Chem. Phys.*, 2006, **124**, 124520.

40 T. Lu and F. Chen, *J. Comput. Chem.*, 2012, **33**, 580-592.

41 W. Humphrey, A. Dalke and K. Schulten, *J. Mol, Graph.*, 1996, **14**, 33-38.

42 M. J. Kamlet, J. L. M. Abboud, M. H. Abraham and R. Taft, *J. Org. Chem.*, 1983, **48**, 2877-2887.

43 Y. Marcus, *Chem. Soc. Rev.*, 1993, **22**, 409-416.

44 L. A. Diverdi and M. R. Topp, *J. Phys. Chem.*, 1984, **88**, 3447-3451.